International Forum on Aeroelasticity and Structural Dynamics
IFASD 2017
25-28 June 2017 Como, Italy

FREEPLAY-INDUCED LIMIT CYCLE OSCILLATION MITIGATION USING LINEAR AND NONLINEAR TUNED VIBRATION ABSORBERS

E. Verstraelen[1], G. Kerschen[1], G. Dimitriadis[1]

[1]Aerospace and Mechanical Engineering Department
Liège University
Allée de la découverte 9, 4000 Liège, Belgium
everstraelen@ulg.ac.be
gdimitriadis@ulg.ac.be

Keywords: IFASD, aeroelasticity, nonlinear, freeplay, NLTVA

Abstract: Structural nonlinearities such as freeplay in control surface bearings and actuators or in connections between wings and external payloads sometimes lead to aeroelastic limit cycle oscillations at airspeeds lower than the linear flutter speed of the aircraft. In parallel, numerous studies demonstrated the potential of linear and nonlinear tuned vibration absorbers to increase the flutter speed of linear and continuously hardening aeroelastic systems such as two-degree-of-freedom wings or long span bridges. In this work, the effect of linear and nonlinear tuned vibration absorbers is studied on a wing with pitch plunge and control surface deflection degrees of freedom and with freeplay in pitch. Depending on the tuning of the linear absorber, the linear flutter speed of the system can be increased by 10% or the onset of limit cycle oscillations due to the freeplay can be delayed by 7.7% and their amplitude can be significantly decreased. The addition of cubic hardening forces on the absorber can further decrease the limit cycle amplitude in a limited airspeed range at the cost of an increase in limit cycle amplitude in another airspeed range. Conversely, the addition of a freeplay hardening force on the absorber can decrease the limit cycle amplitude without any detrimental effect.

1 INTRODUCTION

Structural nonlinearities such as freeplay in control surface bearings and actuators or in connections between wings and external payloads sometimes lead to aeroelastic limit cycle oscillations (LCOs) at airspeeds lower than the linear flutter speed of the aircraft. Such LCOs can reduce maintenance intervals and aircraft performance or even lead to severe structural damage and should therefore be avoided.

One potential way of suppressing these LCOs is the use of passive vibration absorbers. Linear tuned vibration absorbers (LTVAs) have been investigated in civil engineering [1] for flutter suppression however they have received very little attention in the aerospace community. Karpel [2] demonstrated their potential three decades ago on a linear system and several authors studied the effect of such absorbers on systems with hardening nonlinearities [3, 4]. The conclusions of these studies are that such linear absorbers can greatly increase the flutter speed of the system but suffer from a large sensitivity in frequency and that addition of a nonlinear restoring force, resulting in nonlinear tuned vibration absorbers (NLTVAs), can reduce this sensitivity.

In this paper, we propose to investigate the use of such mechanical linear and nonlinear absorbers on a typical aeroelastic system with pitch, plunge and control surface deflection degrees of freedom (DOFs) and with freeplay in pitch. The goal of this work is to delay the onset speed of the LCOs and to reduce their amplitude. This study builds upon previous work on the absorber [3] and on this aeroelastic system [5, 6].

2 AEROELASTIC SYSTEM

The system considered is a classical pitch-plunge-control apparatus made of a 2D symmetric flat plate wing with a control surface. The entire wing, sketched in figure 1(a), is suspended by an extension spring with stiffness K_h and a rotational spring of stiffness K_θ from its pitch axis x_f. These two springs provide restoring forces in the plunge, h, and pitch, θ, DOFs respectively. The control surface deflection angle β is an additional DOF, restrained by a rotational spring with stiffness K_β. The control surface hinge lies at x_h and the total chord of the wing is denoted by c. The inertial, stiffness and damping parameters of this system are set to the values of an experimental apparatus similar to that used by Conner et al [7].

A mechanical NLTVA of mass m_a is attached to the primary system at a distance x_a from the flexural axis by means of a dashpot of damping c_a, a linear spring of stiffness k_a and a nonlinear spring that provides a nonlinear restoring force F_{nl}. Cubic hardening and freeplay springs are considered in this study. The absorber can be tuned by adjusting the stiffness and the damping of the system while the absorber mass and position are set to 4% of the total mass, m, and $0.25 \times c$, respectively. This absorber's displacement is described by means of an additional DOF ξ.

The absorber's natural frequency is given by

$$f_{ltva} = \frac{1}{2\pi}\sqrt{\frac{k_a}{m_a}}$$

while its damping is written as

$$\zeta_{ltva} = \frac{c_a}{2\sqrt{m_a k_a}}$$

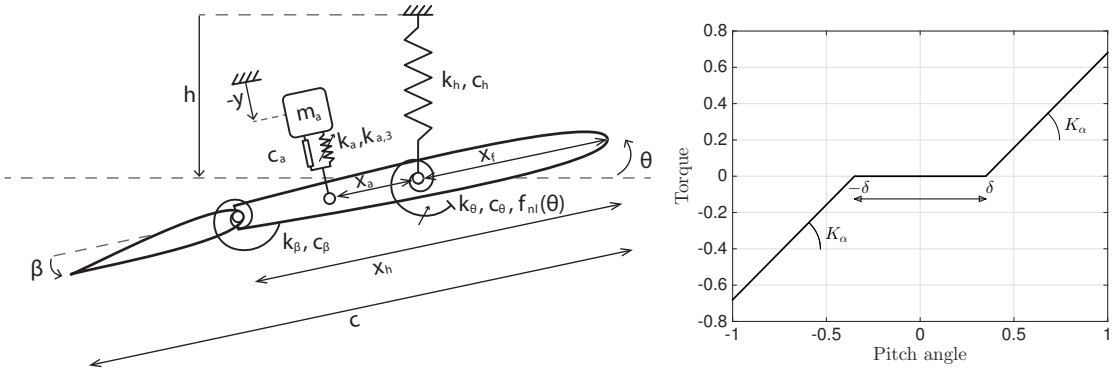

(a) Pitch-Plunge-Control aeroelastic system (b) Freeplay stiffness diagram

Figure 1: Aeroelastic system with freeplay in pitch

It is assumed that there is freeplay in the pitch DOF, such that the restoring force in the corresponding spring is zero while $|\theta| < \delta$, 2δ being the width of the freeplay region. Figure 1(b) shows a typical restoring force diagram for freeplay, whereby the stiffness is K if $|\theta| > \delta$ and zero otherwise. Note that the freeplay region is centred around the origin.

In the case of the pitch-plunge-control wing with freeplay in the pitch DOF, the stiffness outside the freeplay region is given by K_θ, while the stiffness inside the freeplay region is zero. The restoring moment equation is

$$M_\theta(\theta) = \begin{cases} K_\theta(\theta + \delta) & \text{if} \quad \theta < -\delta \\ 0 & \text{if} \quad |\theta| \leq \delta \\ K_\theta(\theta - \delta) & \text{if} \quad \theta > \delta \end{cases} \tag{1}$$

where M_θ is the pitching moment provided by the freeplay spring.

The equations of motion of the system flying with airspeed U in air of density ρ can be developed using linear unsteady attached flow aerodynamic assumptions; a time-domain model can be written by means of Wagner function analysis [7]. The structural displacements are denoted by the vector $\mathbf{y} = [h \quad \theta \quad \beta \quad \xi]$ while the six aerodynamic states are denoted by the vector $\mathbf{w} = [w_1 \quad \dots \quad w_6]$. Then the complete state vector of the system is given by $\mathbf{x} = [\dot{\mathbf{y}} \quad \mathbf{y} \quad \mathbf{w}]^T$ and has dimensions 14×1. The equations of motion of the system coupled with an absorber and with freeplay in the pitch DOF are given by

$$\dot{\mathbf{x}} = \mathbf{Q}_1\mathbf{x} + \mathbf{q}_\theta M_\theta(\theta) + \mathbf{q}_{nl}F_{nl}(\Delta\xi, k_a, c_{nl}) \tag{2}$$

where

$$\begin{aligned}
\mathbf{Q}_1 &= \begin{pmatrix} -\mathbf{M}^{-1}\left(\mathbf{C} + \mathbf{C}_{ltva} + \rho U \mathbf{D}\right) & -\mathbf{M}^{-1}\left(\mathbf{E}_1 + \mathbf{E}_{ltva} + \rho U^2 \mathbf{F}\right) & -\rho U^3 \mathbf{M}^{-1}\mathbf{W} \\ \mathbf{I}_{4\times4} & \mathbf{0}_{4\times4} & \mathbf{0}_{4\times6} \\ \mathbf{0}_{6\times4} & \mathbf{W}_1 & U\mathbf{W}_2 \end{pmatrix} \\
\mathbf{q}_\theta &= \begin{pmatrix} -\mathbf{M}^{-1}\begin{pmatrix} 0 \\ 1 \\ 0 \\ 0 \end{pmatrix} \\ \mathbf{0}_{10\times1} \end{pmatrix} \\
\mathbf{q}_{nl} &= \begin{pmatrix} -\mathbf{M}^{-1}\begin{pmatrix} -1 \\ -x_a \\ 0 \\ 1 \end{pmatrix} \\ \mathbf{0}_{10\times1} \end{pmatrix} \qquad (3) \\
\mathbf{M} &= \mathbf{A} + \mathbf{A}_{ltva} + \rho\mathbf{B} \qquad (4) \\
\Delta\xi &= \theta x_a + h - \xi \qquad (5)
\end{aligned}$$

and $\mathbf{E}_1$, is the value of the structural stiffness matrix inside the freeplay region $\pm\delta$, given by

$$\mathbf{E}_1 = \begin{pmatrix} K_h & 0 & 0 & 0 \\ 0 & 0 & 0 & 0 \\ 0 & 0 & K_\beta & 0 \\ 0 & 0 & 0 & 0 \end{pmatrix} \tag{6}$$

Matrices $\mathbf{A}$, $\mathbf{A}_{ltva}$ and $\mathbf{B}$ are respectively the structural, absorber and aerodynamic mass matrices, $\mathbf{C}$, $\mathbf{C}_{ltva}$ $\rho U\mathbf{D}$ are the structural, absorber and aerodynamic damping matrices respectively. $\mathbf{E}_{ltva}$ and $\rho U^2\mathbf{F}$ are the absorber and aerodynamic stiffness matrices respectively. $\mathbf{W}$ is the aerodynamic state matrix, $\mathbf{W}_1$ and $\mathbf{W}_2$ are the aerodynamic state equation matrices, The notation $\mathbf{I}_{4\times4}$ denotes a unit matrix of size 4×4. The values of all the matrices are given in the appendix. Equation 2 can be written as

$$\dot{\mathbf{x}} = \begin{cases} \mathbf{Q}_1\mathbf{x} + \mathbf{q}_{nl}F_{nl}(\Delta\xi, k_a, c_{nl}) & \text{if} \quad |\theta| \leq \delta \quad \text{(a)} \\ \mathbf{Q}_2\mathbf{x} - \mathbf{q}_\theta K_\theta \operatorname{sgn}(\theta)\delta + \mathbf{q}_{nl}\Delta\xi^3 & \text{if} \quad |\theta| > \delta \quad \text{(b)} \end{cases} \tag{7}$$

where $\mathbf{Q}_2\mathbf{x} = \mathbf{Q}_1\mathbf{x} + \mathbf{q}_\theta K_\theta\theta$.

In this work, we will define two linear sub-systems that are relevant to freeplay:

- Underlying linear system: the system without structural stiffness that is only valid inside the freeplay region (equation 7(a)).
- Overlying linear system: the nominal system without freeplay and with full stiffness (equation 7(b) with δ = 0).

In [5,6], it was demonstrated that such a system can undergo small amplitude two-domain limit cycle oscillations around either extremity of the freeplay range or larger amplitude three-domain limit cycle oscillations that span beyond both ends of the freeplay range. This study focuses on those large amplitude cycles because they usually arise at the same airspeed as the two-domain cycles but their larger amplitude makes them more dangerous.

3 AEROELASTIC ANALYSIS OF THE SYSTEM WITHOUT ABSORBER

Figure 2 depicts the bifurcation diagram of the system without absorber computed using a shooting algorithm [8]. Subfigures 2(a) & 2(c) respectively plot the pitch amplitude variation with airspeed and a close up in the vicinity of the LCO onset speed of the system (lowest airspeed where LCOs can be observed). Subfigures 2(b) & 2(d) respectively display the variation of the LCO frequency and a close up in the vicinity of the LCO onset speed of the system. Finally, subfigures 2(e) & 2(f) correspond to the plunge amplitude and control surface deflection amplitude variation with airspeed. As all the LCOs are symmetric, subfigures 2(c) to 2(f) only depict the positive amplitude. Note that in systems with freeplay, the LCO amplitude depends linearly on the freeplay gap so all the amplitudes are divided by δ.

A symmetric unstable LCO branch arises at $U_{F,0} = 15.67$ m/s, the flutter speed of the underlying system, because of a grazing bifurcation. The continuation code does not reach the grazing point because this unstable branch is very difficult to track close to the freeplay boundary. The unstable branch propagates in the decreasing airspeed direction until $U_{\text{LCO}} = 9.16$ m/s where it folds back and becomes stable. Then, the pitch and control LCO amplitude and the LCO frequency increase rapidly with airspeed while the plunge LCO amplitude decreases then increases until 10.01 m/s where quasi-periodic solutions are observed because of a Neimark-Sacker bifurcation. At airspeeds higher than 11.05 m/s, only stable LCOs are observed, whose amplitude increases smoothly with airspeed and becomes asymptotically infinite at $U_{F,1} = 27.99$ m/s, the flutter speed of the overlying linear system. Small amplitude oscillations can also be observed close to either boundary of the freeplay region however they do not occur at airspeeds smaller

than the large amplitude LCOs studied here and they are less critical because of their small amplitude. Such LCOs are studied in detail in previous papers [5, 6].

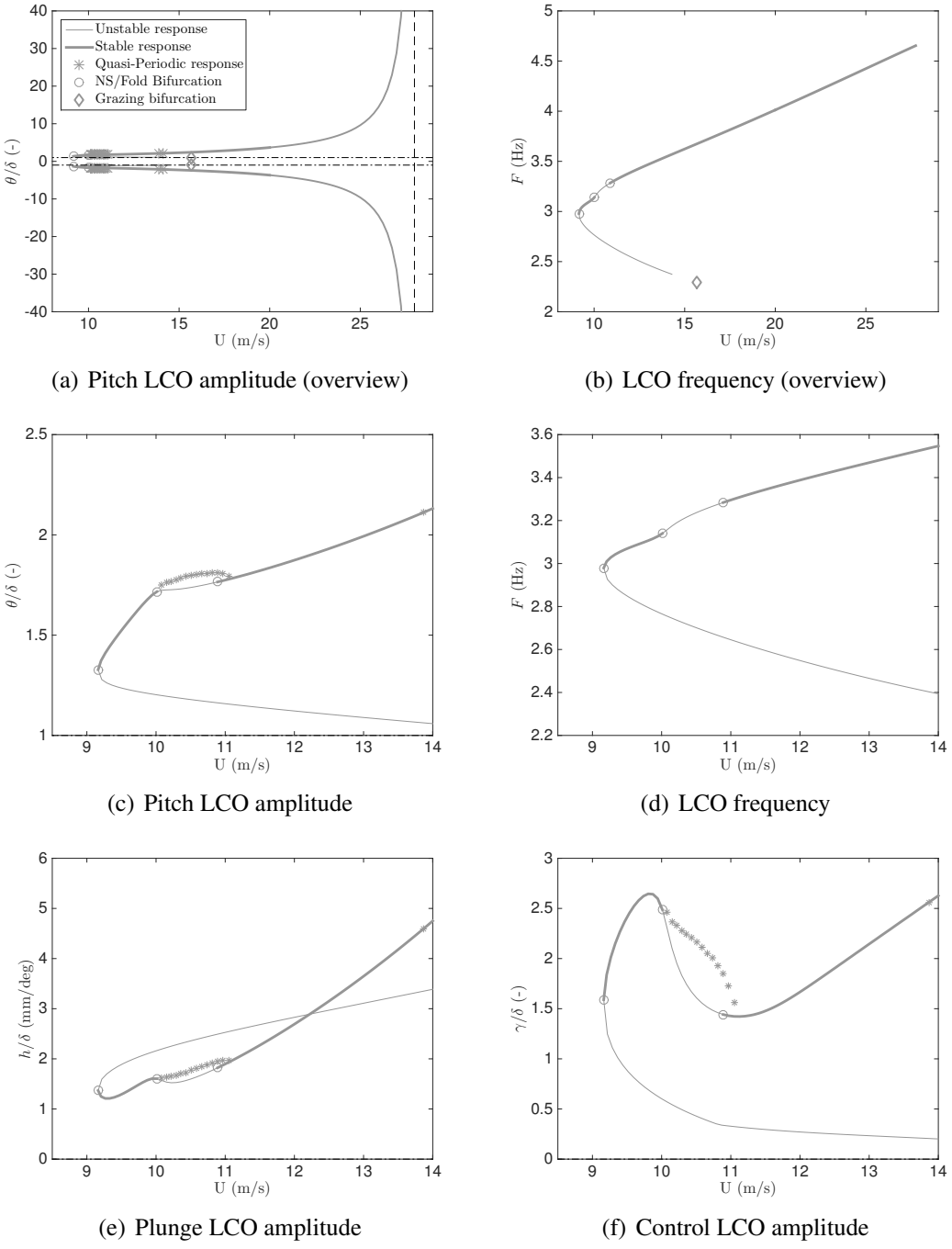

(a) Pitch LCO amplitude (overview)

(b) LCO frequency (overview)

(c) Pitch LCO amplitude

(d) LCO frequency

(e) Plunge LCO amplitude

(f) Control LCO amplitude

Figure 2: Bifurcation diagram of the system without absorber

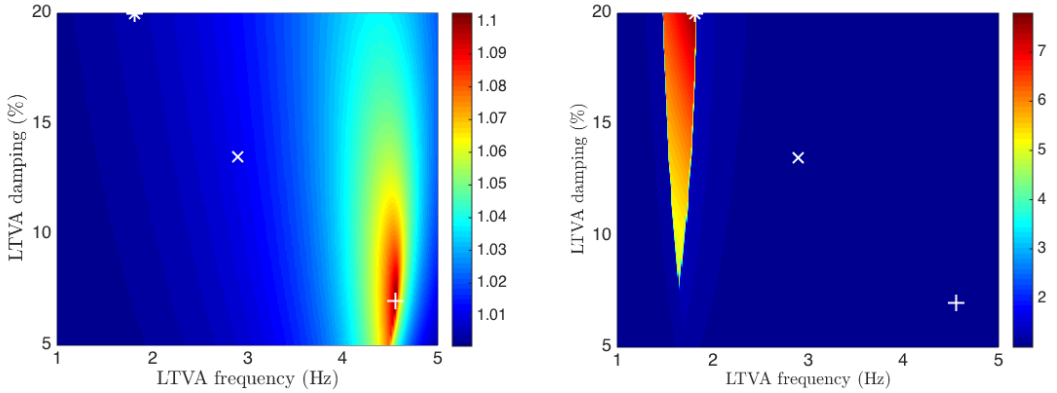

(a) Overlying linear system relative flutter speed (b) Underlying linear system relative flutter speed

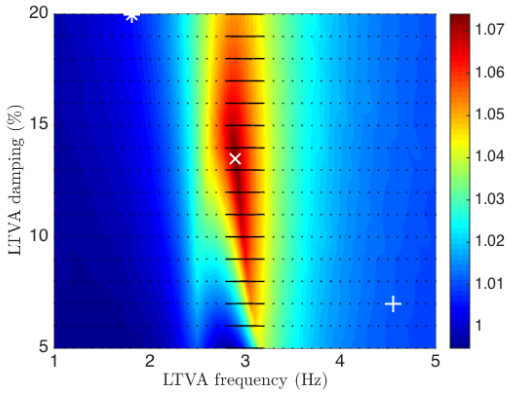

(c) Relative LCO onset speed

Figure 3: Critical airspeeds of the system depending on the absorber tuning

4 EFFECT OF A LINEAR ABSORBER ON THE SYSTEM

4.1 Critical airspeeds optimization

As demonstrated in the previous section, the system without absorber features three critical velocities that one can try to optimise by means of a LTVA. The flutter speed of the underlying linear system, $U_{F,0}$, is the airspeed at which the unstable LCO branch arises because of the grazing bifurcation. The flutter speed of the overlying linear system, $U_{F,1}$, is the flutter speed of the system without freeplay, i.e. in normal operational conditions. Finally, the LCO onset speed, U_{LCO} is the lowest airspeed at which limit cycles can be observed on the system with freeplay. For linear absorbers ($F_{nl} = 0$), the first two airspeeds are linear flutter speeds and can therefore be computed using simple stability analysis while the LCO onset speed is computed from continuation curves similar to those of figure 2 for many absorber configurations.

Figures 3(a) 3(b) and 3(c) respectively plot the relative flutter speed of the overlying linear system, the relative flutter speed of the underlying linear system and the relative LCO onset speed as a function of the LTVA frequency and modal damping.

Each relative airspeed is defined as the ratio of the critical airspeed of the system with absorber to the same critical airspeed of the system without absorber and therefore provides information on the beneficial effect of the absorbers.

-	No LTVA	LTVA 1	LTVA 2	LTVA 3
symbol		$+$	$*$	$\times$
F_{ltva} [Hz]	-	4.56	1.81	2.90
ε_{ltva} [%]	-	7	20	13.5
$U_{F,0}$ [m/s]	15.67	16.68 $(+6.4\%)$	121.24 $(+673\%)$	16.20 $(+3.4\%)$
$U_{F,1}$ [m/s]	27.99	30.86 $(+10\%)$	28.12 $(+0.5\%)$	28.3 $(+1.1\%)$
U_{LCO} [m/s]	9.16	9.31 $(+1.6\%)$	9.26 $(+0.99\%)$	9.87 $(+7.7\%)$

Table 1: Optimal absorber tunings and performance

Each dot of subfigure 3(c) corresponds to one continuation curve while the mesh is not displayed in figures 3(a) and 3(b) because it is much finer. Comparing the three figures shows that a single absorber cannot be tuned to increase all three airspeeds at the same time so three different absorbers are considered; their characteristics and performance are given in table 1. In the tuning region considered, no absorber leads to a decrease in any critical airspeed and a high sensitivity in absorber frequency is observed close to each optimal tuning.

Absorber 1 $(+)$ is optimized for the overlying linear system. It increases the flutter speed of the overlying system by 10%, the grazing airspeed by 6.4% and does not have significant effect on the LCO onset speed.

Absorber 2 $(*)$ is tuned on the underlying linear system. It increases the grazing airspeed by $\approx 673\%$ but has a negligible effect on the LCO onset speed and on the linear flutter speed of the system without freeplay. This suggests that the LCO onset speed is not related to the flutter speed of the underlying linear system.

Absorber 3 $(\times)$ is designed for the full nonlinear system. It increases the LCO onset speed by 7.7% and does not have a significant effect on the overlying and underlying flutter speeds.

4.2 Bifurcation analysis

Figure 4 compares the bifurcation diagram of the system without absorber (grey) to those of absorbers 1, 2 and 3. Subfigures 4(a) to 4(d) respectively correspond to the pitch LCO amplitude, plunge LCO amplitude, control surface deflection LCO amplitude and LCO frequency in the neighbourhood of the LCO onset speed.

Absorber 1 (black) increases the LCO onset speed to 9.31 m/s $(+1.6\%)$, reduces the pitch LCO amplitude between airspeeds 9.31 m/s and 10.76 m/s but has a detrimental effect on the response from 10.76 m/s to 13.01 m/s even though it suppresses the Neimark-Sacker bifurcation. At higher airspeeds, a reduction in LCO amplitude is observed and the airspeed of the vertical asymptote is increased to 30.86 m/s $(+10\%)$, the flutter speed of the overlying linear system. Furthermore, this absorber decreases the LCO frequency.

Absorber 2 (orange) increases the the LCO onset speed to 9.27 m/s $(+0.99\%)$ and slightly reduces the LCO amplitude in all three DOFs. The frequency variation with airspeed is not significantly affected by the absorber. Even though the grazing airspeed is increases by 673%, the LCO onset speed is not significantly increased, which indicates that tuning the absorber on the underlying linear system is not a good option.

Absorber 3 (blue) is optimised for the nonlinear system. The LCO onset speed is increased to 9.87 m/s $(+7.7\%)$ and the LCO amplitude is decreased on all three DOFs. Moreover, the

airspeed range where large amplitude control surface deflection are observed is reduced from $[9.16 - 11.05]$ m/s to $[9.87 - 10.32]$ m/s. Such absorbers also increase the LCO frequency and lead to an abrupt frequency variation with airspeed close to the LCO onset speed.

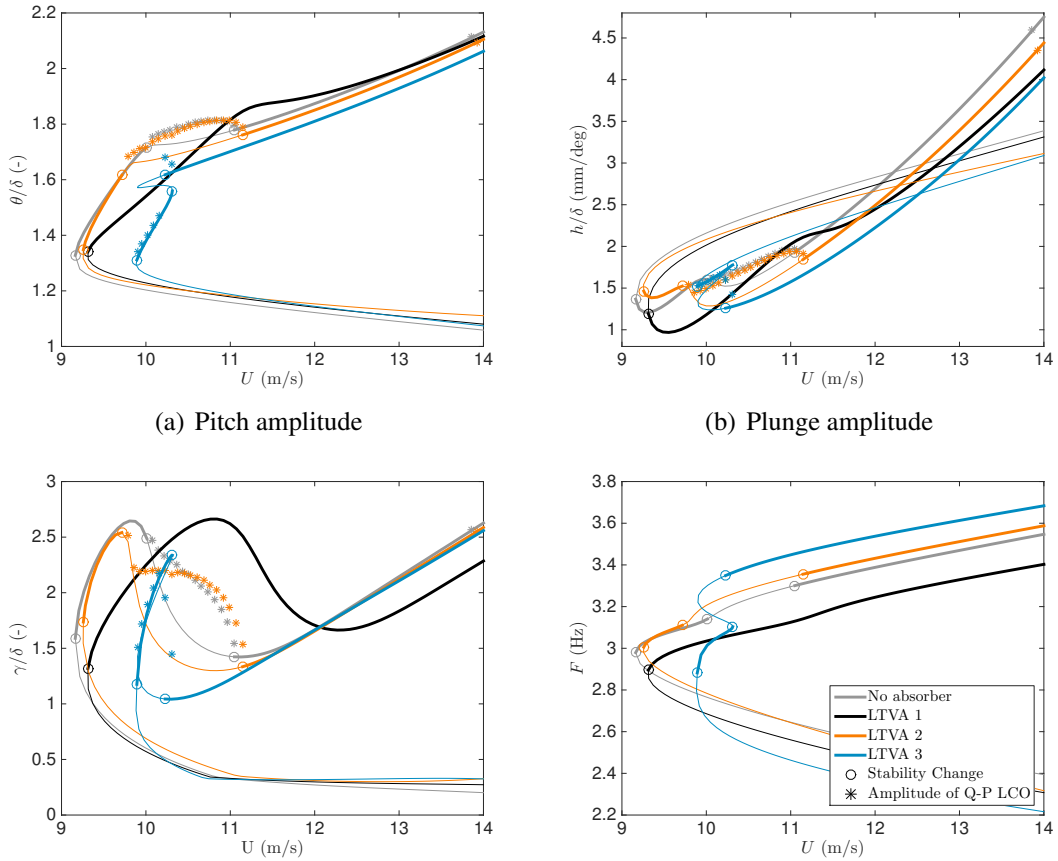

(a) Pitch amplitude

(b) Plunge amplitude

(c) Control amplitude

(d) LCO frequency

Figure 4: Bifurcation diagram of the system with linear absorbers

Figure 5 plots the pitch and plunge LCO amplitude with absorber divided by the LCO amplitude at the same airspeed without absorber, computed from direct simulations. It indicates the reduction in LCO amplitude achieved thanks to the LTVAs. Absorber 1 has a small detrimental effect close to the LCO onset speed then its performance increases with airspeed (and therefore LCO amplitude) because the equivalent stiffness slowly reaches that of the overlying linear system. A reduction in LCO amplitude between 0 and 50% is observed depending on the airspeed. LTVA 2 is not stiff enough for the system and leads to a reduction in LCO amplitude lower than 10% over the whole airspeed region which further indicates that it is not a good option. Absorber 3 offers benefits similar to absorber 1 at high airspeeds but delays the onset speed of the LCOs and has better performance close to the LCO onset speed.

5 EFFECT OF A NONLINEAR ABSORBER ON THE SYSTEM

Linear absorbers are very sensitive to the primary system's frequency which varies with airspeed and amplitude in the present case. A potential option for improving the performance of absorbers in such systems is the addition of a nonlinear restoring force. Habib et al. [9] demonstrated that for optimal performance in forced vibration, the nonlinearity in the absorber should

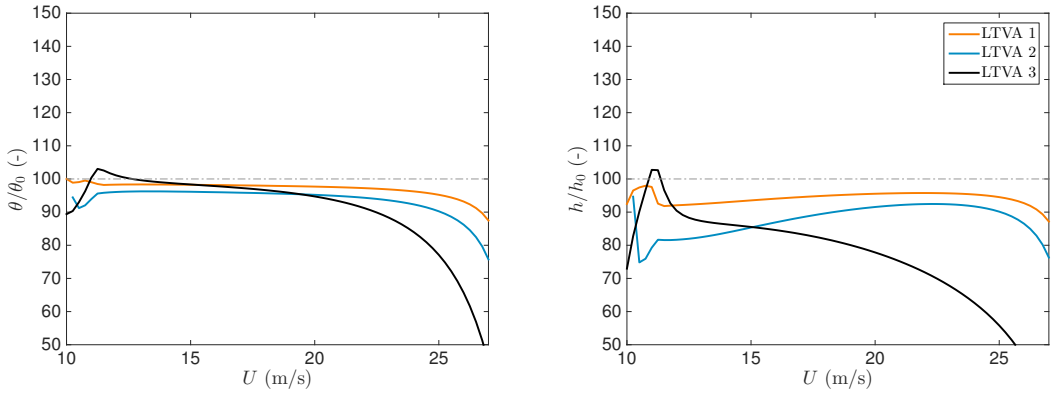

(a) Pitch amplitude ratio

(b) Plunge amplitude ratio

Figure 5: Overview of the performance of the linear absorbers

mimic that of the primary system. In this work, cubic and freeplay nonlinearities are tested and compared. The former nonlinearity is smooth and therefore more simple while the latter respects the principle of similarity. The NLTVAs linear parts are set to the values of LTVA 3 and the goal is to achieve performance similar or higher than LTVA 1 at high speed while maintaining the good performance of LTVA 3 in the vicinity of the LCO onset speed.

5.1 Cubic hardening NLTVA

The cubic NLTVA is an absorber whose linear components are identical to those of LTVA 3 but which also features a cubic hardening spring of restoring force

$$F_{nl}(\Delta\xi) = c_{nl} \times k_a \times \Delta\xi^3 \tag{8}$$

where c_{nl} has to be tuned to achieve the best performance.

Figure 6 plots the bifurcation diagram of the system with four NLTVAs based on LTVA 3. Subfigures 6(a) to 6(d) respectively correspond to bifurcation diagrams in LCO pitch, plunge, and control surface deflection amplitude and in LCO frequency. The grey, orange, blue and black lines respectively correspond to $c_{nl} = 0$, $c_{nl} = 100$, $c_{nl} = 200$ and $c_{nl} = 300$. The thin lines correspond to unstable responses while the thick ones are related to stable solutions.

Previous research on systems with continuous nonlinearities [4, 10] found optimal nonlinear parameters to suppress the sub-criticality that is introduced by the linear absorber in the system. In this more complex system, no clear optimal nonlinear parameter was found. The nonlinearity has a very small effect on the LCO onset speed and each nonlinear parameter has a beneficial effect in one airspeed speed range and a detrimental effect in another.

At airspeeds close to the LCO onset speed, the nonlinearity reduces the rapidity of the pitch, plunge and control surface amplitude growth however it delays the point where the response jumps down to lower levels. This is especially noticeable on the plunge and control surface bifurcation diagrams. At intermediate airspeeds ($12 < U < 20$), all three nonlinear absorbers reduce the LCO amplitude compared to the LTVA and it is very difficult to define an optimal absorber as each absorber is optimal on a given DOF in a given airspeed range. At higher airspeeds ($U > 20$), all three nonlinear absorbers have similar detrimental effect on the response and lead to a LCO amplitude slightly higher than the linear absorber.

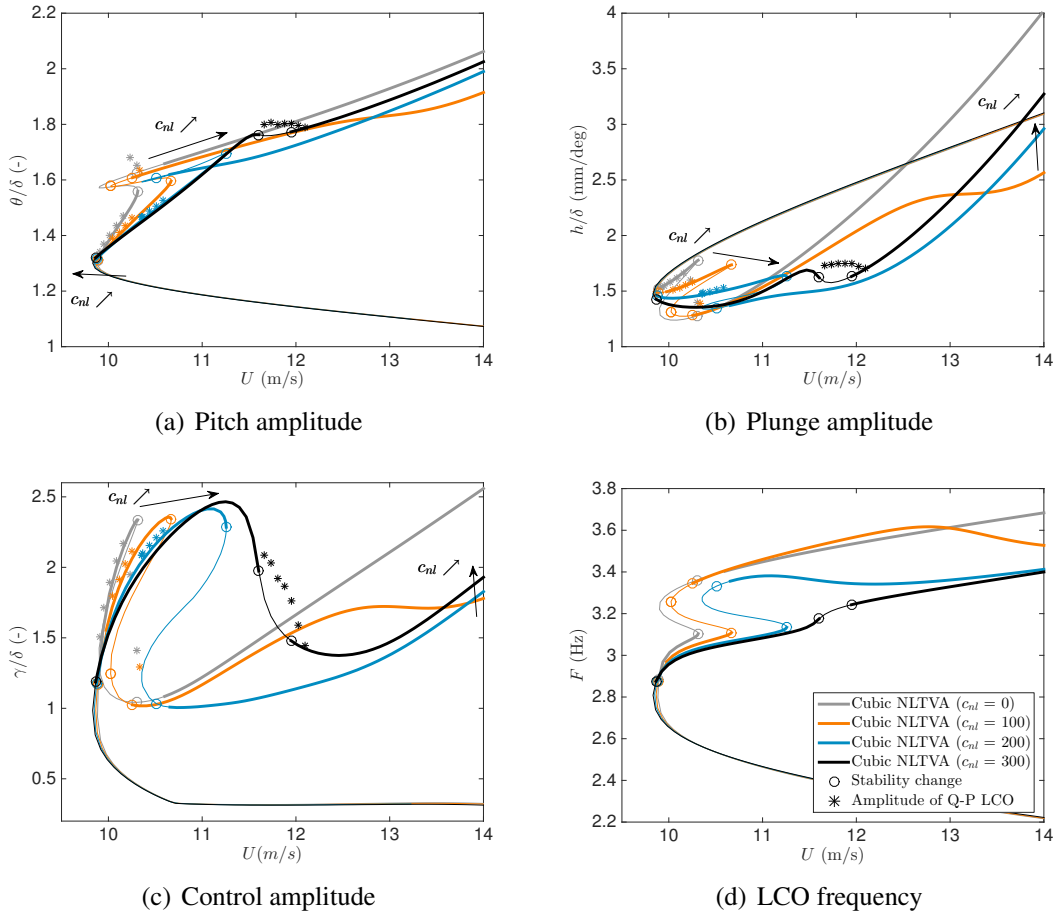

(a) Pitch amplitude (b) Plunge amplitude

(c) Control amplitude (d) LCO frequency

Figure 6: Bifurcation diagram of the system with cubic nonlinear absorbers based on LTVA 3

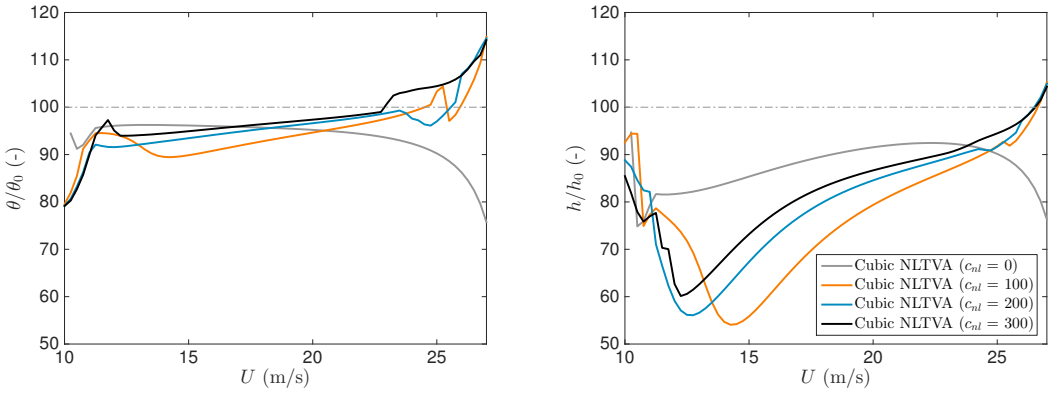

(a) Pitch amplitude ratio (b) Plunge amplitude ratio

Figure 7: Overview of the performance of cubic nonlinear absorbers based on LTVA 3

Figure 7 plots the pitch and plunge LCO amplitude with absorber divided by the LCO amplitude at the same airspeed without absorber, computed from direct simulations. All three nonlinear absorbers offer far better performance than the LTVA on the plunge DOF and slighly better performance than the LTVA at intermediate airspeeds however they have a detrimental effect at small and high airspeeds.

In summary, it is very difficult to draw conclusions on the effectiveness of cubic hardening nonlinear absorbers for freeplay LCO mitigation. All the cases considered improve the behaviour of a given DOF in a given airspeed region at the cost of an increase in LCO amplitude in another airspeed range.

5.2 Freeplay NLTVA

The freeplay NLTVA has all the linear features of LTVA 3 with a nonlinear spring of restoring force given by

$$F_{nl}(\Delta\xi) = \begin{cases} c_{nl} \times k_a \times (\Delta\xi + \Delta\xi_0) & \text{if} \quad \Delta\xi < -\Delta\xi_0 \\ 0 & \text{if} \quad |\Delta\xi| \leq \Delta\xi_0 \\ c_{nl} \times k_a \times (\Delta\xi - \Delta\xi_0) & \text{if} \quad \Delta\xi > \Delta\xi_0 \end{cases} \tag{9}$$

added in parallel to the linear spring of stiffness k_a. The clearance is $\Delta\xi_0$ and the hardening outside the freeplay gap is given by c_{nl}. Note that this nonlinear freeplay spring is attached in parallel to the linear spring of the absorber so the total restoring force is actually bi-linear rather than a real freeplay force.

The first freeplay NLTVA considered is tuned in order to keep the large amplitude control surface deflection region as narrow as with the LTVA. The nonlinear parameters are $\Delta\xi_0 = 0.03$ & $c_{nl} = 1$ (i.e. the stiffness is doubled outside the freeplay range). A second absorber is tuned in order to have an effect similar to that of the cubic absorber with $c_{nl} = 200$ at low airspeeds. The nonlinear parameters of this NLTVA are $\Delta\xi_0 = 0.02$ & $c_{nl} = 0.7$.

Figure 8 plots the bifurcation diagram of the system with the LTVA (grey), with a cubic NLTVA with $c_{nl} = 200$ (blue), with the first freeplay NLTVA (orange) and with the second freeplay NLTVA (black). Subfigures 8(a) to 8(d) respectively correspond to bifurcation diagrams in LCO pitch, plunge, and control surface deflection amplitude and in LCO frequency. The thin lines correspond to unstable responses while the thick ones are related to stable solutions.

The first freeplay NLTVA (black, larger clearance) has a clearance that is not reached close to the LCO onset speed. As a result, the absorber behaves like a LTVA which leads to a rapid increase in pitch LCO amplitude but also keeps the airspeed range where large amplitude control surface deflection oscillations are observed narrow.

The second freeplay NLTVA (orange, smaller clearance) has an effect very similar to that of the cubic hardening absorber close to the LCO onset speed thanks to its small clearance. The main difference is that a small region of quasi-periodic response is observed close to 11 m/s.

Figure 9 plots the pitch and plunge LCO amplitude with absorber divided by the LCO amplitude at the same airspeed without absorber, computed from direct simulations. It shows than the bilinear absorber offers a far better amplitude reduction than the linear and cubic absorbers but also in a much wider airspeed range while maintaining the increase in LCO onset speed. As a result, the proposition of Habib et al. [9] that the nonlinearity in the absorber should mimic that of the primary system appears to be valid for this system. The freeplay NLTVAs considered indeed led to a reduction in LCO amplitude close to the LCO onset speed but also at higher airspeed whereas the cubic NLTVAs led to an increase in LCO amplitude.

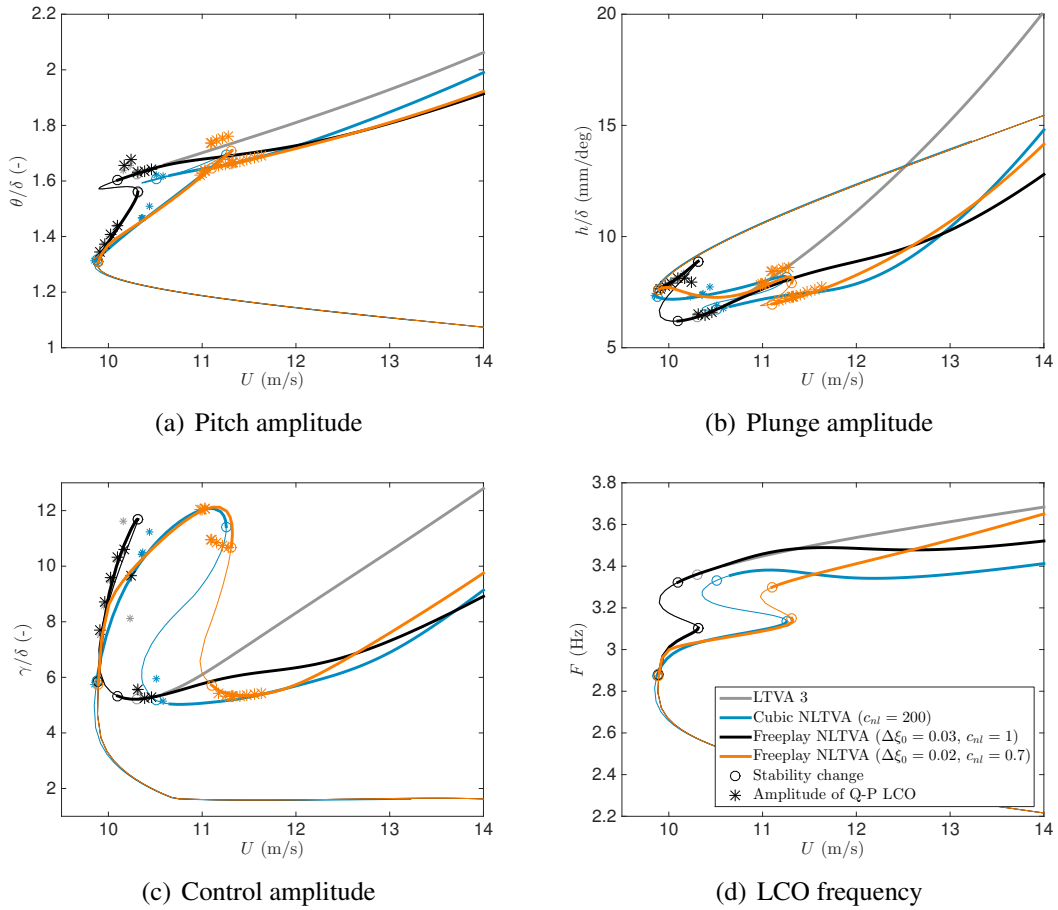

(a) Pitch amplitude (b) Plunge amplitude

(c) Control amplitude (d) LCO frequency

Figure 8: Bifurcation diagram of the system with freeplay and cubic nonlinear absorbers based on LTVA 3

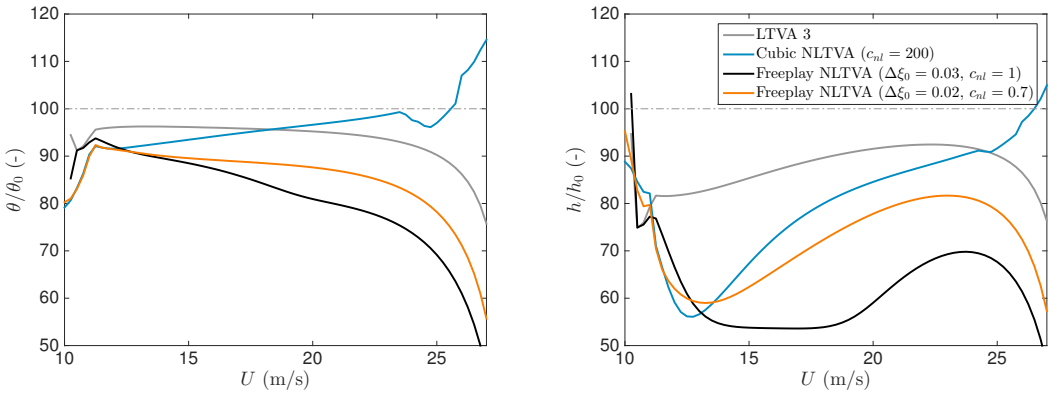

(a) Pitch amplitude ratio (b) Plunge amplitude ratio

Figure 9: Overview of the performance of cubic and bilinear nonlinear absorbers based on LTVA 3

6 CONCLUSION

This study demonstrates that linear tuned vibration absorbers can have a beneficial effect on a wing with pitch, plunge and control surface deflection DOFs, with and without freeplay. The absorbers considered can either increase the flutter speed of the system without freeplay by 10% or delay the LCO onset speed by 7.7% and reduce the LCO amplitude on the nonlinear system but never both at the same time. This mediocre performance compared to other studies [4, 6] is probably due to the increased complexity of the system and to the fact that the absorber considered lies very close to the pitch axis, which limits its effects. Nevertheless, while it is very unlikely to reach typical flutter in real life situations, it is not unlikely to reach a freeplay LCO condition. In such cases, LTVAs 1 and 3 offered a good performance by reducing the LCO amplitude and should therefore not be neglected.

The addition of a cubic nonlinear force to the absorber optimised for the system with freeplay did not further increase the LCO onset speed but led to a substantial reduction in LCO amplitude in a given airspeed region and to an increase in LCO amplitude in another airspeed region irrespective of the value of the nonlinear parameter was chosen. As a result no clear optimal tuning was found and the absorber should be set up depending on the critical airspeed range of the application. Conversely, the addition of a freeplay nonlinear force to the absorber led to a substantial reduction in LCO amplitude in a large airspeed range without any drawback. This is consistent with the prediction of Habib et al. [9] that the nonlinearity in the absorber should mimic the nonlinearity in the primary system.

Several approaches can be followed to further investigate this system and potentially increase the absorber performance. Studying absorbers attached to the control surface or further from the pitch axis should increase the LCO onset speed and linear flutter speed of the system. The freeplay NLTVA was tuned by trial and errors and only based on LTVA 3. Better absorbers (based on LTVA 3 or not) can probably be designed.

7 ACKNOWLEDGEMENTS

The authors would like to acknowledge the financial support of the European Union (ERC Starting Grant NoVib 307265).

8 APPENDIX: AERODYNAMIC AND STRUCTURAL MATRICES OF THE SYSTEM

The matrices appearing in equation 5 are given in the following appendix, while the values of all the parameters are given in table 2.

Structural matrices

The structural inertia matrix is given by

$$\mathbf{A} = \begin{pmatrix} m & S & S_\beta & 0 \\ S & I_\theta & I_{\theta\beta} & 0 \\ S_\beta & I_{\theta\beta} & I_\beta & 0 \\ 0 & 0 & 0 & 0 \end{pmatrix}$$

where $a = x_f/b - 1$, $b = c/2$, $c_h = x_h/b - 1$, $I_{\theta\beta} = I_\beta + b(c_h - a)S_\beta$.

The structural damping matrix is given by

$$\mathbf{D} = \mathbf{V}^{-1^T} \begin{pmatrix} 2\bar{m}_1\omega_1\zeta_1 & 0 & 0 & 0 \\ 0 & 2\bar{m}_2\omega_2\zeta_2 & 0 & 0 \\ 0 & 0 & 2\bar{m}_3\omega_3\zeta_3 & 0 \\ 0 & 0 & 0 & 0 \end{pmatrix} \mathbf{V}^{-1}$$

where $\mathbf{V}$ are the eigenvectors of the matrix $\mathbf{A}^{-1}\mathbf{E}$, $\bar{m}_i$ are the diagonal elements of the matrix $\mathbf{V}^T\mathbf{A}\mathbf{V}$ and ω_i are the square roots of the eigenvalues of the matrix $\mathbf{A}^{-1}\mathbf{E}$.

Finally, the stiffness matrices of the underlying and overlying linear systems are respectively given by

$$\mathbf{E_1} = \begin{pmatrix} K_h & 0 & 0 & 0 \\ 0 & 0 & 0 & 0 \\ 0 & 0 & K_\beta & 0 \\ 0 & 0 & 0 & 0 \end{pmatrix}$$

$$\mathbf{E} = \begin{pmatrix} K_h & 0 & 0 & 0 \\ 0 & K_\theta & 0 & 0 \\ 0 & 0 & K_\beta & 0 \\ 0 & 0 & 0 & 0 \end{pmatrix}$$

LTVA matrices

Assuming small displacements, the inertia, damping and stiffness LTVA matrices are respectively given by

$$\mathbf{A_{ltva}} = m_a \begin{pmatrix} 0 & 0 & 0 & 0 \\ 0 & 0 & 0 & 0 \\ 0 & 0 & 0 & 0 \\ 0 & 0 & 0 & 1 \end{pmatrix}$$

$$\mathbf{C_{ltva}} = c_a \begin{pmatrix} 1 & x_a & 0 & -1 \\ x_a & x_a^2 & 0 & x_a \\ 0 & 0 & 0 & 0 \\ -1 & x_a & 0 & 1 \end{pmatrix}$$

$$\mathbf{E_{ltva}} = k_a \begin{pmatrix} 1 & x_a & 0 & -1 \\ x_a & x_a^2 & 0 & x_a \\ 0 & 0 & 0 & 0 \\ -1 & x_a & 0 & 1 \end{pmatrix}$$

Aerodynamic matrices

The aerodynamic inertia matrix is given by

$$\mathbf{B} = b^2 \begin{pmatrix} \pi & -\pi ab & -T_1 b & 0 \\ -\pi ab & \pi b^2(1/8 + a^2) & -(T_7 + (c_h - a)T_1)b^2 & 0 \\ T_1 b & 2T_{13}b^2 & -T_3 b^2/\pi & 0 \\ 0 & 0 & 0 & 0 \end{pmatrix}$$

The total aerodynamic damping matrix is given by $\mathbf{D} = \mathbf{D}_1 + \Phi(0)\mathbf{D}_2$, where $\Phi(t) = 1 - \Psi_1 e^{-\varepsilon_1 U t/b} - \Psi_2 e^{-\varepsilon_2 U t/b}$ is Wagner's function, with $\Psi_1 = 0.165$, $\Psi_2 = 0.335$, $\varepsilon_1 = 0.0455$, $\varepsilon_2 = 0.3$ and

$$\mathbf{D}_1 = b^2 \begin{pmatrix} 0 & \pi & -T_4 & 0 \\ 0 & \pi(1/2 - a)b & (T_1 - T_8 - (c_h - a)T_4 + T_{11}/2)b & 0 \\ 0 & (-2T_9 - T_1 + T_4(a - 1/2))b & bT_{11}/2\pi & 0 \\ 0 & 0 & 0 & 0 \end{pmatrix}$$

$$\mathbf{D}_2 = \begin{pmatrix} 2\pi b & 2\pi b^2(1/2 - a) & 2\pi b T_{11}/2\pi & 0 \\ -2\pi b^2(a + 1/2) & -2\pi b^3(a + 1/2)(1/2 - a) & -b^3(a + 1/2)T_{11} & 0 \\ b^2 T_{12} & b^3 T_{12}(1/2 - a) & b^3 T_{12} b T_{11}/2\pi & 0 \\ 0 & 0 & 0 & 0 \end{pmatrix}$$

The total aerodynamic stiffness is given by $\mathbf{F} = \mathbf{F}_1 + \Phi(0)\mathbf{F}_2 + \Xi\mathbf{F}_3$ where $\Xi = \Psi_1\varepsilon_1/b + \Psi_2\varepsilon_2/b$ and

$$\mathbf{F}_1 = b^2 \begin{pmatrix} 0 & 0 & 0 & 0 \\ 0 & 0 & (T_4 + T_{10}) & 0 \\ 0 & 0 & (T_5 - T_4 T_{10})/\pi & 0 \\ 0 & 0 & 0 & 0 \end{pmatrix}$$

$$\mathbf{F}_2 = \begin{pmatrix} 0 & 2\pi b & 2bT_{10} & 0 \\ 0 & -2\pi b^2(a + 1/2) & -2b^2(a + 1/2)T_{10} & 0 \\ 0 & b^2 T_{12} & b^2 T_{12} T_{10}/\pi & 0 \\ 0 & 0 & 0 & 0 \end{pmatrix}$$

$$\mathbf{F}_3 = \begin{pmatrix} 2\pi b & 2\pi b^2(1/2 - a) & b^2 T_{11} & 0 \\ -2\pi b^2(a + 1/2) & -2\pi b^3(a + 1/2)(1/2 - a) & -b^3(a + 1/2)T11 & 0 \\ b^2 T_{12} & b^3 T_{12}(1/2 - a) & b^3 T_{12} T_{11}/2\pi & 0 \\ 0 & 0 & 0 & 0 \end{pmatrix}$$

The aerodynamic state influence matrix is given by $\mathbf{W} = [2\pi b\mathbf{W}_0 \quad -2\pi b^2(a+1/2)\mathbf{W}_0 \quad b^2 T_{12}\mathbf{W}_0 \quad \mathbf{0}_{1\times 4}]^T$ where

$$\mathbf{W}_0 = \begin{pmatrix} -\Psi_1(\varepsilon_1/b)^2 \\ -\Psi_2(\varepsilon_2/b)^2 \\ \Psi_1\varepsilon_1(1 - \varepsilon_1(1/2 - a))/b \\ \Psi_2\varepsilon_2(1 - \varepsilon_2(1/2 - a))/b \\ \Psi_1\varepsilon_1(T_{10} - \varepsilon_1 T_{11}/2)/\pi b \\ \Psi_2\varepsilon_2(T_{10} - \varepsilon_2 T_{11}/2)/\pi b \end{pmatrix}$$

The aerodynamic state equation matrices are given by

$$\mathbf{W}_1 = \begin{pmatrix} 1 & 0 & 0 & 0 \\ 1 & 0 & 0 & 0 \\ 0 & 1 & 0 & 0 \\ 0 & 1 & 0 & 0 \\ 0 & 0 & 1 & 0 \\ 0 & 0 & 1 & 0 \end{pmatrix}$$

$$\mathbf{W}_2 = \begin{pmatrix} -\varepsilon_1/b & 0 & 0 & 0 & 0 & 0 \\ 0 & -\varepsilon_2/b & 0 & 0 & 0 & 0 \\ 0 & 0 & -\varepsilon_1/b & 0 & 0 & 0 \\ 0 & 0 & 0 & -\varepsilon_2/b & 0 & 0 \\ 0 & 0 & 0 & 0 & -\varepsilon_1/b & 0 \\ 0 & 0 & 0 & 0 & 0 & -\varepsilon_2/b \end{pmatrix}$$

The T_1-T_{14} coefficients are defined in Theodorsen [11] and many other classic aeroelasticity texts.

	Wing dimensions	
Chord (with flap)	c	25.4 cm
Span	s	52 cm
Flexural axis	x_f	$0.25 \times c$
	Flap dimensions	
Chord (flap alone)	$-$	6.25 cm
Span	s_2	52 cm
Hinge axis	x_h	$0.75 \times c$
	Inertial parameters	
Plunge mass	m	2.562 kg
Pitch inertia	I_θ	0.0181 m.kg
Control inertia	I_β	2.6610^{-4} m.kg
Pitch static imbalance	S	0.0943 m.kg
Pitch-Flap inertia product	$I_{\theta,\beta}$	0.0013 m.kg
Flap static imbalance	S_β	0.0084 m.kg
	Stiffness parameters	
Plunge stiffness	K_h	850.7 N/m
Pitch stiffness	K_θ	34 Nm/rad
Flap stiffness	K_β	1.512 Nm/rad
	Absorber parameters	
Mass ratio	$\overline{m}_a$	4%
Mass	m_a	$\overline{m}_a \times m$
Position	x_a	$0.25c$
Stiffness	k_a	optimised
Damping	c_a	optimised
Nonlinear stiffness	$k_{a,3}$	optimised
	Modal parameters	
Plunge mode frequency	f_1	2.9 Hz
Pitch mode frequency	f_2	7.1 Hz
Control mode frequency	f_3	17.0 Hz
Plunge mode damping	ζ_1	0.87%
Pitch mode damping	ζ_2	1.39%
Flap mode damping	ζ_3	0.6%

Table 2: Structural parameters of the experimental system

9 REFERENCES

[1] Gu, M., Chang, C., Wu, W., et al. (1998). Increase of critical flutter wind speed of long-span bridges using tuned mass dampers. *Journal of Wind Engineering and Industrial Aerodynamics*, 73(2), 111–123.

[2] Karpel, M. (1981). *Design for active and passive flutter suppression and gust alleviation*, vol. 3482. National Aeronautics and Space Administration, Scientific and Technical Information Branch.

[3] Verstraelen, E., Habib, G., Kerschen, G., et al. (2016). Experimental passive flutter suppression using a linear tuned vibration absorber. *AIAA Journal*, 1–16. doi: 10.2514/1.J055397.

[4] Malher, A., Touzé, C., Doaré, O., et al. (2017). Flutter control of a two-degrees-of-freedom airfoil using a nonlinear tuned vibration absorber. *Journal of Computational and Nonlinear Dynamics*, –.

[5] Dimitriadis, G. (2015). Asymmetric limit cycle oscillations in systems with symmetric freeplay. In *Proceedings of the International Forum on Aeroelasticity and Structural Dynamics*, IFASD-2015-009. St Petersburg, Russia.

[6] Verstraelen, E., Dimitriadis, G., Rossetto, G. D. B., et al. (2017). Two-domain and three-domain limit cycles in a typical aeroelastic system with freeplay in pitch. *Journal of Fluids and Structures*, 69, 89 – 107. ISSN 0889-9746. doi: https://doi.org/10.1016/j.jfluidstructs.2016.11.019.

[7] Conner, M. D., Tang, D. M., Dowell, E. H., et al. (1997). Nonlinear behaviour of a typical airfoil section with control surface freeplay: a numerical and experimental study. *Journal of Fluids and Structures*, 11(1), 89–109.

[8] Dimitriadis, G. (2017). *Introduction to Nonlinear Aeroelasticity*. John Wiley & Sons, Ltd. ISBN 9781118756478, pp. 313–388. doi:10.1002/9781118756478.ch7.

[9] Habib, G. and Kerschen, G. (2016). A principle of similarity for nonlinear vibration absorbers. *Physica D: Nonlinear Phenomena*, 332, 1 – 8. ISSN 0167-2789. doi: http://dx.doi.org/10.1016/j.physd.2016.06.001.

[10] Habib, G. and Kerschen, G. (2016). Passive flutter suppression using a nonlinear tuned vibration absorber. *Nonlinear Dynamics, Volume 1: Proceedings of the 33rd IMAC, A Conference and Exposition on Structural Dynamics, 2015*, 133–144.

[11] Theodorsen, T. (1935). General theory of aerodynamic instability and the mechanism of flutter. Tech. Rep. NACA TR-496, NACA.

COPYRIGHT STATEMENT